ARCTIC SEA ICE MAPPING USING SENTINEL-1 SAR SCENES WITH A CONVOLUTIONAL NEURAL NETWORK

Dmitrii Murashkin[1,2,3], *Anja Frost*[2]

1. Center for Industrial Mathematics, University of Bremen, Bremen, Germany
2. German Aerospace Center (DLR), Bremen, Germany
3. Institute of Environmental Physics, University of Bremen, Bremen, Germany

murashkin@uni-bremen.de

ABSTRACT

In this paper we focus on automated sea ice mapping based on satellite images with deep learning methods. We adjust the UNET++ convolutional neural network architecture for sea ice type semantic segmentation and create a per-pixel classifier for Sentinel-1 SAR scenes. The classification is done tile-wise, i.e. a Sentinel-1 scene is divided into tiles, classified, and then the results are joined back to form the classified scene. We address to the border effect appearing when a tiled classification is applied.

Index Terms— sea ice, SAR, Sentinel-1, classification, semantic segmentation, CNN, UNET++

1. INTRODUCTION

A map of sea ice types is of a great importance for ships operating in the Arctic. Information on sea ice situation in the surrounding of a ship is very limited. Ice radar installed on ships helps to choose the path through sea ice, but it has limited range and does not allow to make strategic decisions. Synthetic Aperture Radar (SAR) is an active instrument operating in microwave frequencies that is able to provide radar backscatter information about the ocean and ice surfaces all year round, independently on weather conditions and presence of daylight. The resolution of satellite SAR systems can reach 1 meter, but often a courser resolution is used to increase the spatial coverage. Despite its advantages, the use of satellite SAR images onboard of ships operating in the Arctic is limited due large image size (and low internet bandwidth in high-altitude areas). Also, information in microwave spectrum is harder to interpret compared to optical images. Thus, a regional sea ice map would be a helpful tool for ship route planning.

In the previous studies several methods to derive additional information for SAR image analysis were used. One of the traditional methods is the use of image texture features based on gray level co-occurrence matrix (GLCM). It has been applied for general classification of underlying surface in the original study [1]. GLCM features has been applied for sea ice – open water discrimination [2, 3], and sea ice type classification [4, 5]. With development of SAR techniques, it became possible to acquire images in quadro-polarization mode. This allowed development of methods based on polarimetric features. Polarimetric features were successfully applied for iceberg detection [6, 7], melt pond fraction estimation [8, 9] and sea ice type classification [10, 11].

Convolutional Neural Network (CNN) is one of the supervised deep learning methods often used for image classification and segmentation. In traditional image analysis methods image features (texture features based on GLCM, polarimetric features, band ratios, etc.) are predefined and calculated prior to the training procedure. Apart of these methods, a CNN calculate and adjust image features during the training process to get a feature set, that is best for the description of input images for a given task.

In our study we apply the UNET++ convolutional neural network architecture for per-pixel sea ice classification. Per-pixel classification is often referred to as semantic segmentation.

2. SEA ICE CLASSIFICATION ALGORITHM

2.1. Sentinel-1 Data

Sentinel-1 is a constellation of two identical satellites carrying a Synthetic Aperture Radar (SAR) instrument each. The radar operates in C-band (5.4 GHz) and provides radar images of the Earth surface year round, independently of weather conditions or presence of sunlight. Over open ocean, measurements are done in the Extra Wide swath mode providing dual-band (HH and HV) scenes with 400 km swath width and 40 m pixel size. Sentinel-1 scenes are available on the Copernicus Open Access Hub.

Our preprocessing chain for Sentinel-1 data is shown in Figure 1. First, we calibrate scenes to γ_0 with the auxiliary

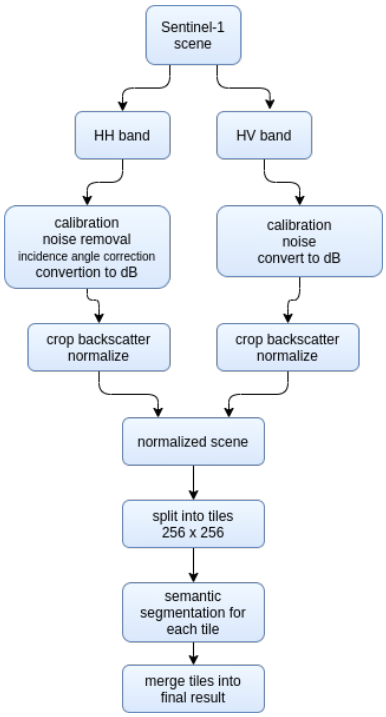

Fig. 1. Data flow scheme. The HH and the HV bands are preprocessed separately and normalized to [-1; 1]. Then the bands are stacked together and split into tiles. Tiles are classified and merged to the final result.

noise and calibration data provided. After that, an incidence angle correction derived from scenes taken over sea ice is applied to HH band. We cut out backscatter values below -32 dB (noise level), values above 4 dB for HH band and above -16 dB for the HV band. Next, we apply a 5-pixel size bilateral filter to reduce speckle noise. Then the scene is normalized to [-1; 1] range. The normalized scene is cut into 256-pixel tiles with an offset when needed (see Section 2.4) and is passed to a convolutional neural network.

2.2. Sea Ice Types and Training Dataset

We create a training set by manual labeling Sentinel-1 scenes. The following surface types typical for Arctic winter are recognized and labeled:

- multiyear ice - sea ice that has survived at least one summer; this class often represents thick and rough ice
- first-year ice - ice of 30 cm to 1.5 m thickness that might contain ridges
- new ice - newly forming thin ice with thickness up to 30 cm; this class includes gray and white-gray ice
- leads and open water that has low surface roughness; might contain areas covered with nilas (1-2 cm thick ice forming under calm weather conditions)

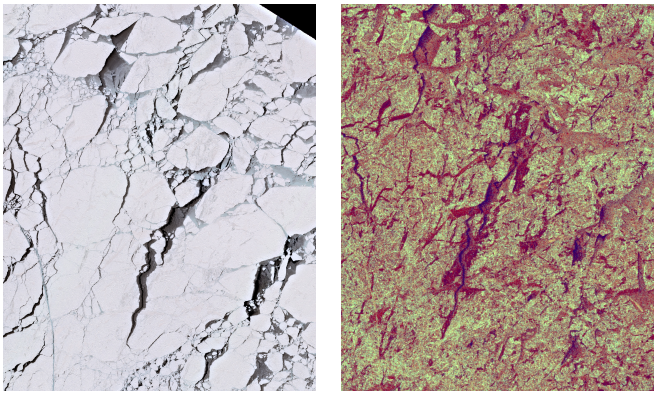

(a) (b)

Fig. 2. (a) Optical Sentinel-2 image (RGB); (b) Sentinel-1 SAR image in pseudocolor: R - HH band, G - HV band, B - band ratio. Scenes are taken in the Fram Strait area on 31 March 2019 with about 8 hours time difference between Sentinel-1 and Sentinel-2 acquisitions.

- leads and open water with wind-roughened surface
- rough ice - includes areas of crushed ice floating in the water, frost flowers, and might contain ridges.

Whenever Sentinel-2 optical data is available, we use it to evaluate the labeling. Figure 2 shows an example in which both Sentinel-1 SAR and Sentinel-2 optical data are available. Both images were taken on 31 March 2019 in the Fram Strait, the time difference between scenes is about 8 hours.

In total we use seven Sentinel-1 scenes taken in January 2020 as the training dataset. These scenes are cut into 256-pixel tiles to produce a dataset for training. To reduce border effects, we mark eight border pixels of each tile as unlabeled.

2.3. Convolutional Neural Network

For our sea ice classification we use UNET++ convolutional neural network architecture described by [12]. This architecture is a encoder-decoder network where encoder and decoder are connected on each level. Apart from the "traditional" UNET, it allows to combine features at different scales at the final classification layer. The CNN architecture we use is shown in Figure 3. We increased the depth of the encoder (the left part of the scheme) to six layers. The depth of the decoder (the right part of the scheme) is four layers and is smaller than the depth of the encoder. This means that classified images have four time lower resolution compared to corresponding input Sentinel-1 scenes.

2.4. Tiling Edge Effects

Whenever a large image has to be split into tiles to apply a classification, edge effects appear at the border between adja-

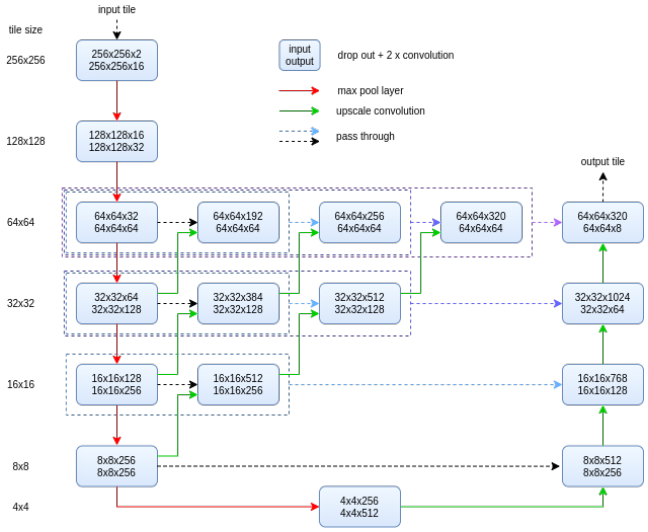

Fig. 3. CNN architecture based on UNET++ architecture. The decoder (red arrows) has a depth of six layers, whereas the encoder part (green arrows) has four layers. The column on the left shows the tile size at each depth level. Numbers in boxes show the input and the output tensor shapes.

cent tiles. To deal with this effect, we include two techniques that reduce the influence of near-border pixels on the classification result.

The first one is applied before the model training. We set four near-border pixels of the label images as "unlabeled". To do this, we create an extra class for unlabeled pixels and set the weight of the class equal to zero, so that the presence of this class does not influence the loss value during the model training process.

The second technique is applied as a postprocessing step of the classification. The trained model is applied to a single scene four times. Each time the input scene is cut into tiles with an offset as shown in Figure 4. Black, red, green, and blue colors correspond to 0% (no offset), 25%, 50%, and 75% relative offset. Then each pixel of a classified tile is weighted linearly by its distance from an edge. In this way a pixel in a middle of a tile has higher weight and therefore higher probabilities compared to a pixel at an edge. After that, the four probabilities (one per offset) for each class are summed up, and the pixel class is chosen based on the maximal class probability value. For example, a pixel (shown as a violet point) of an input scene will appear in the middle of the red tile (25% offset tiling), closer to edge of the green tile (50% offset tiling) and the black tile (no offset tiling), and at the edge of the blue tile (75% offset tiling). Therefore, class probabilities, produced by the model applied to the red tile, will have the highest contribution to the final result, and class probabilities, produced by the model applied to the blue tile, will have the lowest contribution. Thus, the influence of near-border pixels on the per-pixel classification result is decreased, improving the final classification result as the transition between tiles becomes smooth.

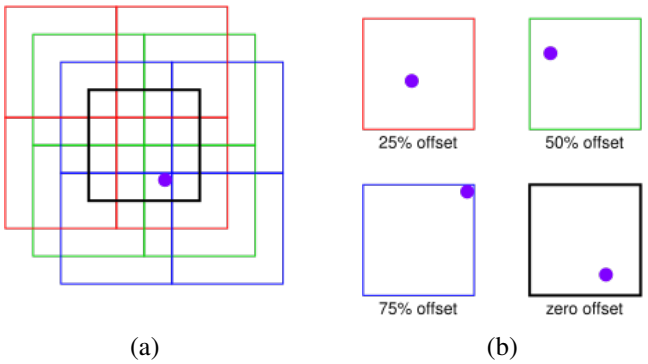

Fig. 4. Scheme for smooth prediction that reduced edge effects. Trained model is applied to a given scene four times, each time with an offset. Zero offset is shown in black, 25% offset is red, 50% offset is green, 75% offset is blue. A pixel of a tile (shown in violet) appears close to the center of the tile in case of red tiling and close to the edge on the blue tiling.

3. RESULTS

The model is trained using 90% of the training dataset, the rest 10% are used as test data during the training procedure to prevent overfitting. The training process is stopped when the last 30 epochs do not improve (decrease) the loss score on the test data. Accuracy of the trained model is 97.6% on the training data and 96.2% on the test data. The accuracy values above do not take into account the smooth classification technique described in Section 2.4.

Results of the classification applied to a Sentinel-1 scene taken in the Beaufort Sea is shown in Figure 5. The upper image shows the pseudocolor Sentinel-1 scene: red - HH band, green - HV band, blue - band ratio. The lower image represents a sea ice map that corresponds to the Sentinel-1 image above. MYI stands for multiyear ice, FYI is first-year ice class. New ice and rough ice classes include ice types described in Section 2.2. Two lead classes correspond to smooth surface leads and rough surface leads as described above. We found a good correspondence of the classified image with the original Sentinel-1 scene. Edge effects appearing due to tiling are not noticeable on the resulting image.

4. REFERENCES

[1] Robert M. Haralick, K. Shanmugam, and Its'hak Dinstein, "Textural Features for Image Classification," *IEEE Transactions on Systems, Man, and Cybernetics*, vol. smc-3, no. 6, pp. 610–621, 1973.

[2] Natalia Yu Zakhvatkina, Vitaly Yu Alexandrov, Ola M.

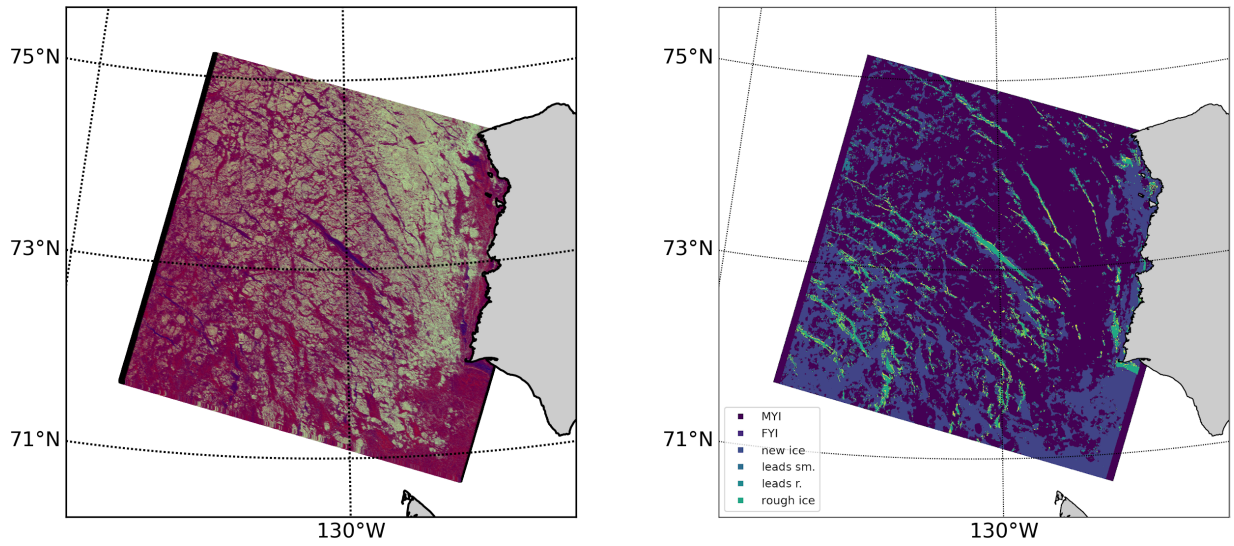

Fig. 5. (a) Sentinel-1 scene taken in the Beaufort Sea, pseudocolor: red - HH, green - HV, blue - band ratio; (b) Sea Ice map produced from the scene above with the trained model: MYI - multiyear ice, FYI - first-year ice, two lead classes for smooth and rough surfaces (as described in Section 2.2)

Johannessen, Stein Sandven, and Ivan Ye Frolov, "Classification of sea ice types in ENVISAT synthetic aperture radar images," *IEEE Transactions on Geoscience and Remote Sensing*, vol. 51, no. 5, pp. 2587–2600, 2013.

[3] Dmitrii Murashkin, Gunnar Spreen, Marcus Huntemann, and Wolfgang Dierking, "Method for detection of leads from Sentinel-1 SAR images," *Annals of Glaciology*, vol. 59, no. 76, pp. 124–136, 2018.

[4] Leen-kiat Soh, Costas Tsatsoulis, and Senior Member, "Texture Analysis of SAR Sea Ice Imagery," *IEEE Transactions on Geoscience and Remote Sensing*, vol. 37, no. 2, pp. 780–795, 1999.

[5] Huiying Liu, Huadong Guo, and Lu Zhang, "SVM-Based Sea Ice Classification Using Textural Features and Concentration From RADARSAT-2 Dual-Pol ScanSAR Data," *IEEE Journal of Selected Topics in Applied Earth Observations and Remote Sensing*, 2015.

[6] Wolfgang Dierking and Christine Wesche, "C-band radar polarimetry - Useful for detection of icebergs in sea ice?," *IEEE Transactions on Geoscience and Remote Sensing*, vol. 52, no. 1, pp. 25–37, 2014.

[7] Vahid Akbari and Camilla Brekke, "Iceberg detection in open and ice-infested waters using C-Band polarimetric synthetic aperture radar," *IEEE Transactions on Geoscience and Remote Sensing*, vol. 56, no. 1, pp. 407–421, 2018.

[8] R. K. Scharien, K. Hochheim, J. Landy, and D. G. Barber, "First-year sea ice melt pond fraction estimation from dual-polarisation C-band SAR - Part 2: Scaling in situ to Radarsat-2," *Cryosphere*, vol. 8, no. 6, 2014.

[9] Ane S. Fors, Dmitry V. Divine, Anthony P. Doulgeris, Angelika H.H. Renner, and Sebastian Gerland, "Signature of Arctic first-year ice melt pond fraction in X-band SAR imagery," *Cryosphere*, vol. 11, no. 2, pp. 755–771, 2017.

[10] Rudolf Ressel, Suman Singha, Susanne Lehner, Anja Rosel, and Gunnar Spreen, "Investigation into Different Polarimetric Features for Sea Ice Classification Using X-Band Synthetic Aperture Radar," *IEEE Journal of Selected Topics in Applied Earth Observations and Remote Sensing*, vol. 9, no. 7, pp. 3131–3143, 2016.

[11] Suman Singha, Malin Johansson, Nicholas Hughes, Sine Munk Hvidegaard, and Henriette Skourup, "Arctic Sea Ice Characterization Using Spaceborne Fully Polarimetric L-, C-, and X-Band SAR with Validation by Airborne Measurements," *IEEE Transactions on Geoscience and Remote Sensing*, vol. 56, no. 7, pp. 3715–3734, 2018.

[12] Zongwei Zhou, Md Mahfuzur Rahman Siddiquee, Nima Tajbakhsh, and Jianming Liang, "UNet++: Redesigning Skip Connections to Exploit Multiscale Features in Image Segmentation," *IEEE Transactions on Medical Imaging*, vol. 39, no. 6, pp. 1856–1867, 2020.